European Journal of Pharmaceutical Sciences 188 (2023) 106521

Contents lists available at ScienceDirect

European Journal of Pharmaceutical Sciences

journal homepage: www.elsevier.com/locate/ejps

# Critical nanomaterial attributes of iron-carbohydrate nanoparticles: Leveraging orthogonal methods to resolve the 3-dimensional structure

Leonard Krupnik [a,b,c], Prachi Joshi [d], Andreas Kappler [d,e], Beat Flühmann [f], Amy Barton Alston [f], Reinaldo Digigow [f,*], Peter Wick [a], Antonia Neels [b,c]

[a] Laboratory for Particles-Biology Interactions, Materials meet Life, Swiss Federal Laboratories for Materials Science and Technology (Empa), St. Gallen, Switzerland
[b] Center for X-ray Analytics, Materials meet Life, Swiss Federal Laboratories for Materials Science and Technology (Empa), St. Gallen, Switzerland
[c] Department of Chemistry, University of Fribourg, Fribourg 1700, Switzerland
[d] Geomicrobiology, Department of Geosciences, University of Tuebingen, Tuebingen 72076, Germany
[e] Cluster of Excellence: EXC 2124: Controlling Microbes to Fight Infection, Tuebingen 72076, Germany
[f] CSL Vifor, Flughofstrasse 61, Glattbrug 8152, Switzerland

ARTICLE INFO

*Keywords:*
Iron-carbohydrate complex
Orthogonal
Physicochemical characterization
Mössbauer
SAXS
SANS
Biorelevance

ABSTRACT

Intravenous iron-carbohydrate nanomedicines are widely used to treat iron deficiency and iron deficiency anemia across a wide breadth of patient populations. These colloidal solutions of nanoparticles are complex drugs which inherently makes physicochemical characterization more challenging than small molecule drugs. There have been advancements in physicochemical characterization techniques such as dynamic light scattering and zeta potential measurement, that have provided a better understanding of the physical structure of these drug products in vitro. However, establishment and validation of complementary and orthogonal approaches are necessary to better understand the 3-dimensional physical structure of the iron-carbohydrate complexes, particularly with regard to their physical state in the context of the nanoparticle interaction with biological components such as whole blood (i.e. the nano-bio interface).

## 1. Introduction

Iron deficiency is a global health problem that is associated with a wide variety of underlying etiologic conditions including chronic kidney disease, heart failure, underlying inflammatory conditions, cancer, bariatric surgery as well as menorrhagia and post-partum bleeding (Cappellini et al., 2020). Iron is a key driver for erythropoiesis and formation of red blood cells but it is also a critical element in cellular processes including mitochondrial energy metabolism (Richards et al., 2021). Many of the diseases associated with iron deficiency are chronic and require repeated doses of iron supplementation (Cappellini et al., 2020). Intravenous iron-carbohydrate products were developed to circumvent the challenges of gastrointestinal tolerability of oral iron salts such as ferrous sulfate which can result in poor patient adherence (Auerbach and Ballard, 2010). Early studies evaluating intravenous administration of mononuclear and polynuclear iron as well as ferric oxide demonstrated significant, unacceptable toxicity risks (Goetsch and Moore, 1946). Drug design and development programs resulted in carefully designed carbohydrate ligands that were complexed and bonded to polynuclear iron cores to produce iron-carbohydrate nanoparticles (Funk and Barton, 2021). These products were then able to furnish their pharmacologic activity more safely and effectively when delivered intravenously (Funk and Barton, 2021). After intravenous administration, it is presumed that the iron-carbohydrate complex is taken up by circulating macrophages and delivered to the mononuclear phagocytic system where the complexes are biodegraded via mechanisms that have not yet been elucidated (Funk et al., 2022). However, it has been shown that each iron-carbohydrate product demonstrates its own unique iron biodistribution profile in animal models (Funk et al., 2022). In human subjects, the pharmacokinetic profile for total serum iron and pharmacodynamic profile for serum ferritin has also been shown to be distinct between products with different carbohydrate ligands and surface characteristics (Garbowski et al., 2020). There have also been publications of small case series demonstrating difference in clinical performance when an originator iron-carbohydrate complex (iron sucrose) was switched with a follow-on and vice versa, despite products having comparable specifications described in regulatory guidance (Aguera et al., 2015; Rottembourg et al., 2011; US_FDA

* Corresponding author.
*E-mail address:* reinaldo.digigow@viforpharma.com (R. Digigow).

https://doi.org/10.1016/j.ejps.2023.106521
Received 19 January 2023; Received in revised form 8 June 2023; Accepted 6 July 2023
Available online 8 July 2023

**Table 1**
Recommended Factors for Assessment of Nanomaterial from US Food and Drug Administration's (FDA) guidance for drug products, including biological products, that contain nanomaterials.

| | |
|---|---|
| 1 | Adequacy of characterization of the material structure and its function. |
| 2 | Complexity of the material structure. |
| 3 | Understanding of the mechanism by which the physicochemical properties of the material impact its biological effects (e.g., effect of particle size on pharmacokinetic parameters). |
| 4 | Understanding the in vivo release mechanism based on the material's physicochemical properties. |
| 5 | Predictability of in vivo release based upon established in vitro release methods. |
| 6 | Physical and chemical stability. |
| 7 | Maturity of the nanotechnology (including manufacturing and analytical methods). |
| 8 | Potential impact of manufacturing changes, including in-process controls and the robustness of the control strategy on critical quality attributes (CQAs) of the drug product. |
| 9 | Physical state of the material upon administration. |
| 10 | Route of administration. |
| 11 | Dissolution, BA, distribution, biodegradation, accumulation and their predictability based on physicochemical parameters and animal studies. |

September 2021).

While the development of iron-carbohydrate products advanced treatment of iron deficiency and iron deficiency anemia, regulatory evaluation of these nanomedicines remains challenging due to their relatively small particle size and overall complexity (Nikravesh et al., 2020). The production of iron-carbohydrate complexes is highly sensitive to manufacturing process conditions such as pH, temperature, and reagents used as well as production scales, presenting challenges to reproducible manufacturing of the final drug product (Nikravesh et al., 2020; US_FDA 2022). Importantly, the critical quality attributes (CQAs) for iron-carbohydrate nanomedicines have not been formally established, particularly with regard to the surface structures which are heterogeneous between the approved products. Thus, at present, physicochemical characterization alone cannot fully reduce residual uncertainty when assessing sameness between an innovator and follow-on product. The US Food and Drug Administration's (FDA) guidance for drug products containing nanomaterials provides eleven factors that are crucial to making a risk-based evaluation of these drug products (Table 1) (US_FDA 2022). The agency has recognized the fundamental role of physicochemical characterization in points 1 and 2 (Table 1) as well as the necessity to fully understand the CQAs in order to understand the linkage of these characteristics to in vivo disposition as identified in points 3, 4, 5 and 11 (US_FDA 2022; Marden et al., 2018). Acknowledging the complexity of the iron carbohydrates and the criticality of any manufacturing changes, the European Medicines Agency published a reflection paper in 2015 that supports the potential utility of additional testing for comparability of iron-carbohydrate complexes including use of orthogonal analytic techniques (European_Medicines_Agency 2015). This reflection paper also refers to the requirements outlined in the International Council for Harmonisation's guidance (CPMP/ICH/5721/03) on biotechnological/biological products that are subject to changes based on their manufacturing process (Agency, 2005). Both the FDA and EMA's guidance documents are not formally binding, however, they do give valuable insight to the challenges the scientific community has raised in regard to evaluating iron-carbohydrate nanomedicines

Despite being used in clinical practice for decades, the in vivo biodisposition profiles and mechanisms of biodegradation of the iron carbohydrate in the mononuclear phagocytic system (MPS) are not established (Funk et al., 2022). The FDA and the scientific community recommend orthogonal methods to characterize components of complex drug products (US_FDA 2022; Simon et al., 2023). There are many analytical methods that can be utilized to evaluate the physical structure of the whole, intact iron-carbohydrate nanoparticle and the polynuclear iron core. There are also some established methods to evaluate the carbohydrate ligand, however, this is an area where more intensive research is needed due to the obvious biological (e.g., immune system, serum proteins) interactions with the carbohydrate ligand (Dobrovolskaia, 2022; Monopoli et al., 2011). This underscores the need to further develop physicochemical characterization methods that can further elucidate important structural features of these nanomedicines that will be predictive of in vivo performance (Mahmoudi, 2021).

There are emerging techniques that augment an orthogonal approach to characterization methods that can then be used collectively to deepen the understanding of the iron-carbohydrate nanoparticle characteristics that ultimately influence the nano-bio interface. Only when a fully validated complement of characterization methods is established, can studies of more biorelevant test methods (e.g., in vitro release testing, in vitro to in vivo correlation and physiologically based pharmacokinetic models) be explored for regulatory evaluation of this complex class of drugs. This review will contextualize various analytical methods, both long- established and those with newer applications, to evaluate the physical structure of the intact iron-carbohydrate complex, the iron core and the carbohydrate ligand in the framework of comparative evaluation of drug products.

## 2. Challenges with physicochemical evaluation of iron-carbohydrate nanoparticles

Iron-carbohydrate nanoparticle products are complex drugs (Wu et al., 2017). This class of drugs has also been referred to as non-biological complex drugs or NBCDs as they share complex features of their physical attributes with biological drug products including heterogeneous structures and product stability challenges (Fluhmann et al., 2019). Importantly, the commercially available iron-carbohydrate drug products are comprised of colloidal solutions of the iron-carbohydrate nanoparticles that are quite concentrated and exhibit a demonstrative black/brown color that can interfere with assay techniques that involve spectrophotometric readout (Funk et al., 2022; Garbowski et al., 2020; Pai, 2015). Dilution of these products beyond approved prescribing information label requirements also compromises the stability of these colloidal solutions (Lee et al., 2013; Di Francesco et al., 2019). The particle sizes of the available iron-carbohydrate products are also quite small compared to other approved nanomedicines and range from approximately 8 to 24 nm (Funk and Barton, 2021). Notably, their physicochemical properties are also likely affected through interaction with the complex biomolecular environment including plasma protein adsorption, however, these interactions have not been well characterized to date (Funk and Barton, 2021; Monopoli et al., 2011).

Despite this review focusing on contextualization of various analytical methods that can be used together to best characterize the physical structure of the intact iron-carbohydrate complex, the iron core and the carbohydrate ligand, it is central to also point out the importance of the full chemical characterization of the carbohydrates and the impurities such as low molecular weight iron and free iron species, labile iron, iron II, elemental impurities and other drug substance (DS) and drug product (DP) manufacturing process related substances and potential degradation products.

## 3. Analysis of the whole, intact iron-carbohydrate nanoparticle

Dynamic Light Scattering (DLS) is the most common method for the determination of the particle size of nanoparticles, and it is a method recommended by the regulators for the size characterization of iron-carbohydrate nanoparticles (US_FDA September 2021; US_FDA 2022; European_Medicines_Agency 2015). The size information is given by the hydrodynamic diameter (or radius) and particle size distribution (PSD). DLS measures fluctuations in scattered light intensity caused by the Brownian motion of nanoparticles and calculates the particle

hydrodynamic diameter via the correlation function and the Stokes–Einstein equation (Lim et al., 2013; Gioria et al., 2018; Caputo et al., 2019; Varenne et al., 2016; Mehn et al., 2017; Anderson et al., 2013).

In comparison to other techniques (e.g., transmission electron microscopy, atomic force microscopy) used to measure the particle size of the whole iron-carbohydrate nanoparticles, the DLS method is the most straightforward technique in terms of sample preparation, analysis time and costs. It can be easily incorporated into the in-process control of the manufacturing process, quality control (QC) and to check the colloidal stability of the nanoparticle formulations that might undergo significant aggregation or degradation during storage. However, the results can be affected by the experimental conditions and the method has some limitations for the analysis of polydisperse samples. Iron-carbohydrate nanoparticle samples normally require dilution to minimize absorbance of laser light and multiple scattering events. This means that the sample has to be diluted before analysis, which reduces the scattering signal and thus, without proper method validation the dilution can increase the possibility of error of the measurements. DLS has also only been validated for the intact iron-carbohydrate complex (Di Francesco and Borchard, 2018). In order to measure the hydrodynamic diameter of the polynuclear iron core alone with DLS, pH-controlled dialysis must be used to remove most of the carbohydrate ligand. However, this may induce agglomeration of iron cores, which would give particle sizes that do not represent the drug product administered to patients.

Other techniques such as Size Exclusion Chromatography (SEC) (Süß et al., 2018; Zou et al., 2017; Held and Kilz, 2021). Asymmetric Flow Field Flow Fractionation (AF4) (Wagner et al., 2014; Yohannes et al., 2011). Particle Tracking Analysis (NTA) (Maguire et al., 2018). Analytical Ultracentrifugation (AUC) (Caputo et al., 2019; Schuck et al., 2015; Walter et al., 2014) or Tunable Resistive Pulse Sensing (TRPS) (Weatherall and Willmott, 2015) can also be used for the characterization of the size and particle size distribution of nanoparticles in general. Nevertheless, these techniques have also their limitations, and this might need to be taken in consideration when choosing these methods for the characterization of iron-carbohydrate nanoparticles.

Fundamentally, DLS as well as the other techniques can determine size parameters and colloidal stability only of the whole iron-carbohydrate nanoparticle but are not able to discriminate between structural features of the carbohydrate ligand and the iron core (Jahn et al., 2011).

## 4. Polynuclear iron core

For characterization of the iron core size, cryogenic transmission electron microscopy (Cryo-TEM) and atomic force microscopy (AFM) can be used. The TEM principle is based on the transmission of an electron beam through a sample, so the transmitted electrons that interact with this sample can be used to form an image (Titus et al., 2019). In the case of iron-carbohydrate nanoparticles, the electrons coming from the electron beam are absorbed, transmitted or scattered by the iron cores, which have a higher electron density when compared to the carbohydrate ligands. So, the contrast image in bright-field mode appears dark for the core and bright for the carbohydrate ligands forming the image of the cores (Wu et al., 2016). The instrument uses an objective lens for focusing and magnification of the images (Titus et al., 2019). The TEM technique, especially high-resolution instruments, allows imaging at an atomic level and determination of the crystallographic structure of nanoparticles (Titus et al., 2019). For iron-carbohydrate nanoparticles, Cryo-TEM is demonstrated to be a more appropriat technique when compared with room temperature TEM. In Cryo-TEM, samples are prepared in liquid nitrogen avoiding sample dehydration and consequently introduction of artifacts such as aggregation, and thus more accurate images of the iron cores are generated (Wu et al., 2016). However, caveats of TEM are laborious sample preparation, selection bias caused by choosing from a large number of images as well as the system not being measured in solution conditions. The ability to perform in-situ studies to simulate in vivo environments is hence rather limited. Additionally, structural features of the carbohydrate ligand cannot be determined due to a lack of contrast when using common staining protocols. Other methods like AFM can give insights on the size of iron formulations in all three dimensions both in solution and in a powder state. In AFM, the sample is measured by using a small cantilever with a sharp tip to scan its surface. The contact of the tip and the sample's surface causes small deflections in the cantilever and consequently a slight change in the direction of a laser beam, which is reflected into a photosensitive photodiode detector. The image of the sample's surface topography is created by scanning the area of interest. So, the deflection of the cantilever, which is influenced by the features on the sample surface, is monitored by the photodiode detector, thus creating a three-dimensional visualization of the sample (Titus et al., 2019). Although it has been shown that vertical height and lateral diameter of iron-carbohydrate nanoparticles can be measured, results were highly dependent on sample concentration, scan mode and shape of the probe (Kudasheva et al., 2004). Hence, it was concluded that AFM may not be a reliable technique for determining the size of iron-carbohydrate nanoparticles.

Another method which enables the estimation of iron core size is X-ray diffraction (XRD). XRD can be used for the characterization of crystal structure and crystallite size of iron colloids. The technique is based on the principle of Bragg's equation ($2d \sin\theta = n\lambda$). Bragg diffraction occurs when X-rays of the wavelength $\lambda$ are scattered in a specular fashion by the atoms of a crystalline system, and undergo constructive interference. For a crystalline solid, the waves are scattered from lattice planes separated by the distance $d$ between layers of atoms. Constructive interference of waves occurs only at definite angles $\theta$, measured from the surface normal; $n$ is the diffraction order (1st, 2nd, 3rd,…). The effect of constructive or destructive interference intensifies based of the cumulative effect of reflection in successive crystallographic (diffraction) planes of the crystalline lattice. By measuring the broadness of the observed diffraction peaks from crystalline samples in powders or suspensions, the mean coherence length can be determined, which in the case of iron-carbohydrate nanoparticles, matches the size of iron core. In this regard, the size of nano-crystallites can be derived using the Scherrer (Monshi, 2012) or the Williamson-Hall approach (Suryanarayana and Grant Norton, 1998). One major disadvantage of XRD when handling iron-carbohydrate nanoparticles is a high contribution of amorphous background to the diffraction pattern which is also caused by the carbohydrate ligand. However, this amorphous part of the sample can, at least partly, be removed by pH-adjusted dialysis (Kudasheva et al., 2004).

## 5. Carbohydrate ligand

Zeta potential is the most common parameter used to describe the surface charge of colloidal nanoparticles. The principle of zeta potential measurements is similar to gel electrophoresis, where an electric field is applied to a sample and the charged particles start to move because of their interaction with the electric field. When nanoparticles are exposed to an electric field, the oppositely charged counterions present in the sample form an inner layer around the particles' so-called Stern layer, then around this layer a second layer is formed consisting of both opposite and same charged ions. This diffuse layer is formed because of the electrostatic field of the charged particles, and it is very dynamic and can be affected by concentration, pH and ionic strength of the dispersion medium. The two layers are called the electric double layer (EDL). The zeta potential is defined by the electric potential difference between the EDL attached to the dispersed particles and the dispersion medium (Zou et al., 2017; Titus et al., 2019; Bhattacharjee, 2016; Carvalho et al., 2018). Similar to DLS, zeta potential is a straightforward technique in terms of sample preparation, analysis time and cost. The measurement of the charge of the particles is very important because of its correlation to the interaction with proteins in biological medium and cell uptake

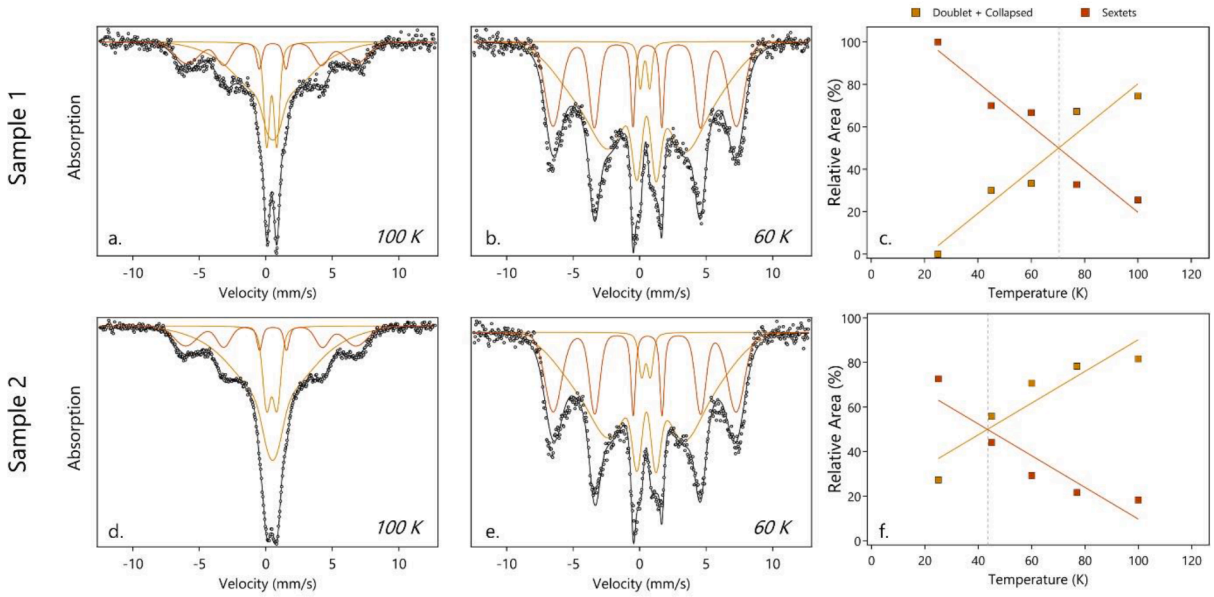


**Fig. 1.** Comparison of two iron-saccharate samples by $^{57}$Fe Mössbauer spectroscopy
Examples of Mössbauer spectra collected at different temperatures (a, b, d, e) and the resulting areas (c, f) for two iron-carbohydrate samples. In a, b, d, e, the black markers denote the data, the black line denotes the total fit, the orange line denotes the doublets and collapsed sextets, and the red line denotes the sextets. The doublets and collapsed features are considered together as they represent the fraction of the sample that is unordered or partially magnetically ordered, while the sextets represent the fraction of the sample that is fully ordered. In c and f, the relative areas of the doublets and collapsed sextet and the sextets are shown as square markers, based on fits to spectra collected at 25 K, 45 K, 60 K, 75 K, and 100 K (of which a subset is shown in a, b, d, e). The solid lines denote linear regressions of the relative areas of the doublets + collapsed sextets phase and the sextets phase. The intersection of the two lines, i.e., temperature at which the relative abundances of the two phases are equal, is the blocking temperature, indicated by the dashed gray line.

mechanisms. The drawback is the fact that iron-carbohydrate nanoparticles can be very sensitive to measurement conditions and sample preparation. The results can be affected by diluent properties (e.g., pH, ionic strength and concentration) and size dispersity of the particles. Therefore, the validation of the analytical methods is very important, and especially for comparative studies, the samples need to be measured under the same conditions. Because zeta potential does not give any information about the possible interactions of carbohydrate ligands and iron cores and neither the ratios of bound/unbound ligand, additional techniques such as Nuclear Magnetic Resonance (NMR), Size-exclusion chromatography (SEC), Thermal Gravimetric Analysis (TGA), Differential scanning calorimetry (DSC) and Fourier Transform Infrared Spectroscopy (FTIR) are necessary to complement the characterization of the carbohydrate ligand.

## 6. Improving biorelevance using orthogonal methods

### 6.1. Mössbauer spectroscopy

Mössbauer spectroscopy is a powerful analytical tool to characterize the speciation of the iron core (Enver Murad, 2004). This spectroscopic technique utilizes the Mössbauer effect, according to which certain nuclides undergo recoil-free, resonant absorption and emission of energy, specifically gamma rays (Mössbauer, 1958). This effect can be prominently observed in $^{57}$Fe nuclei, making Mössbauer spectroscopy an useful technique to probe the nuclear environment of iron nuclei.

Based on $^{57}$Fe Mössbauer spectroscopy, the binding environment of iron, specifically the (i) oxidation state, and (ii) mineralogy can be determined. A typical Mössbauer spectrum consists of peaks grouped together as two, referred to as a doublet, or six, named a sextet. The parameters of these doublets and sextets indicate the iron species and their relative areas correspond to their abundance. For example, the Mössbauer spectrum of some clay minerals such as chlorite contains two doublets with distinct parameters that correspond to Fe(II) and Fe(III) in the phyllosilicate structure (Coey, 1984). Based on the relative areas of the two doublets in the spectrum, the relative proportion of Fe(II) and Fe (III) can be determined. Further, sextets in the Mössbauer spectrum exhibit distinct parameters characteristic of different crystalline iron minerals such as iron (oxyhydr)oxides, which can be used for quantitative identification. Such quantitative identification has been illustrated in environmental samples such as soils and synthetic samples such as ferric carboxymaltose particles. (e.g., Thompson et al., 2011; Neiser et al., 2015).

The collection of spectra at several temperatures offers additional insight into the crystallinity of the Fe species in a given sample. All iron minerals exhibit magnetic behavior. The majority of iron minerals undergo magnetic ordering at characteristic temperatures that are referred to as the Curie temperature, which depends on mineral crystallinity. Magnetic ordering of iron phases is apparent in the appearance of sextets in Mössbauer spectra as the measurement temperature is lowered. A classic example of this transition is the poorly crystalline iron(III) hydroxide mineral 2-line ferrihydrite (nominally $Fe(OH)_3$) that exhibits a paramagnetic doublet at temperatures above 77 K. As the temperature is lowered, splitting of the doublet into a sextet can be observed. At 5 K, the spectrum exhibits a sextet instead of a doublet, indicating magnetic ordering (Byrne and Kappler, 2022). The magnetic ordering of iron minerals with a decrease in temperature has been used in the past to quantify the abundance of poorly crystalline iron(III) (oxyhydr)oxides relative to crystalline iron(III) (oxyhydr)oxides and to determine the role of organic matter for iron mineral transformation (ThomasArrigo et al., 2018; Thompson et al., 2006) and the effect of trace element substitution on mineral crystallinity (Latta et al., 2012; Murad, 1984).

The analysis of Fe speciation described above is applicable to the characterization of the iron core within nanoparticulate iron-carbohydrate complexes. Based on doublets and/or sextets within the spectrum of a particular iron carbohydrate sample, the oxidation state of iron can be determined. By collecting spectra at a range of temperatures, the relative areas of doublets and sextets can be quantified. The temperature at which the relative areas of doublets and sextets are equal, i.e., 50% of the sample is magnetically ordered, can then be calculated.

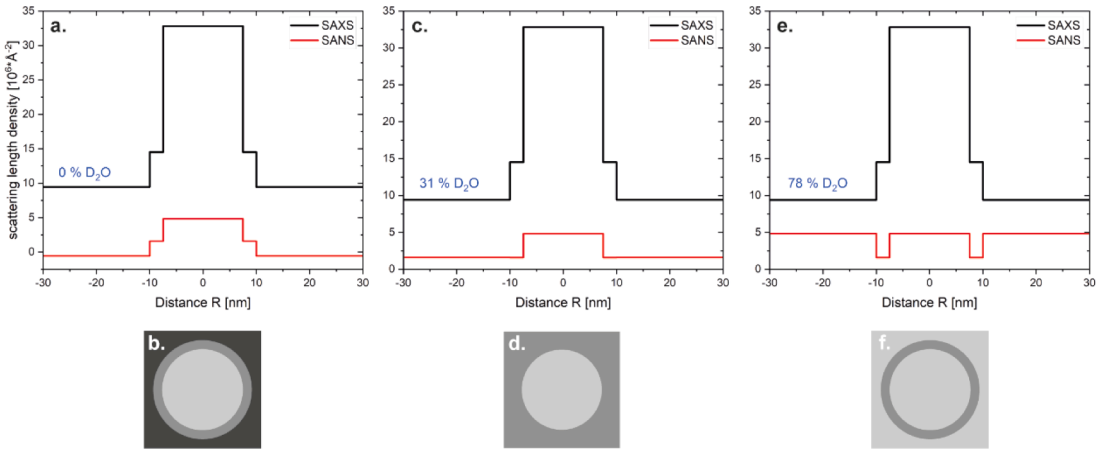


**Fig. 2.** Difference in scattering length density (SLD) profiles between SAXS and SANS for an iron-carbohydrate complex. Figure adapted and modified from A Rübe et al., 2005 (ThomasArrigo et al., 2018).
(a) Full dissolution of the complex in $H_2O$ does not enable high contrast (difference between $SLD_{shell}$ and $SLD_{solvent}$) on the carbohydrate shell due to the substantially higher contrast (difference between $SLD_{core}$ and $SLD_{solvent}$) of the iron core in both SAXS and SANS. This is schematically represented in (b) indicating the SLD of the iron core, carbohydrate shell and solvent as different gray shades. (c) Increasing the concentration of heavy water ($D_2O$) compared to $H_2O$ to 31% during a SANS experiment enables the highest contrast on the iron core as the carbohydrate shell is matched with the solvent as schematically respresented in (d). (e) Increasing the concentration of heavy water ($D_2O$) further to 78% during a SANS experiment enables the highest contrast on the carbohydrate shell as the iron core is matched with the solvent as schematically represented in (f).

This temperature, referred to as the blocking temperature, can be compared between samples to compare their crystallinity. Samples of higher crystallinity have higher blocking temperatures, i.e., they order at higher temperatures (Fig. 1). In the measurement of two iron-carbohydrate samples, the blocking temperature of Sample 1 is higher (70.3 K) relative to that of Sample 2 (43.4 K), indicating that Sample 1 is more crystalline than Sample 2 (Fig. 1c, f).

### 6.2. *Small-angle x-ray scattering (SAXS) and small-angle neutron scattering (SANS)*

Small-angle x-ray scattering (SAXS) is a method that can determine structural information such as size, size distribution, shape and surface properties of nanoscale materials. Samples can be solid or liquid, amorphous or crystalline, and their structure can be resolved in the range of 1 to 100 nm (Schnablegger, 2013; Pauw, 2014). SAXS is a non-destructive, label-free technique, which usually requires no special sample preparation and can be applied to a plethora of nanoparticulate systems including lipids and lipid nanoparticles (Parra-Ortiz et al., 2020; Hassett et al., 2021; Aljuaid et al., 2021), polymers (Jouault et al., 2010; Räntzsch V et al., 2019), microemulsions (Amirkhani et al., 2014; Mahrhauser et al., 2015), metal nanoparticles (Doblas et al., 2019), (coated) metal oxide nanoparticles (Doblas et al., 2019; Huang et al., 2019; Appel et al., 2019; Grünewald et al., 2015) as well as biological materials (Rasmussen et al., 2022; Lenton et al., 2021). It is based on the elastic scattering of X-rays when travelling through a material, recording their scattering at small angles. Since all nano-objects of a given sample are illuminated over all orientations simultaneously, SAXS measurements always provide an average representation of the nanoscale structure, which makes the method resistant to selection bias. Contrast in SAXS is highly dependent on the atomic number and volume of the particles, which means that large objects are easier detected compared to small objects. To achieve maximum contrast, the electron density of the surrounding matrix should be as different as possible from the electron density of the investigated nanomaterial.

Small-angle neutron scattering (SANS) is a technique that allows the characterization of structures at the nanoscale ranging from 1 to 100 nm. Similar to SAXS, it can extract information about the average size, size distribution, shape and spatial arrangement between specific structural features of a nanomaterial (Hammouda, 2008). Its main advantage compared to SAXS is its ability to vary the contrast of specific structural features of a nanomaterial. As SANS uses neutrons instead of X-rays, contrast does not depend on the atomic number but rather on the isotope. This fundamental difference in the scattering process enables the characterization of structures, which are difficult to investigate with both SAXS and TEM. For instance, organic coatings on the surface of nanoparticles can be analyzed efficiently with SANS (Diroll et al., 2015). Contrast enhancement can be achieved by varying the scattering length density of the solvent through control of the concentrations of light water ($H_2O$) and heavy water ($D_2O$) (Fig. 2) (Rübe et al., 2005). High concentrations of $D_2O$ improve the contrast for organic materials like a carbohydrate ligand (Fig. 2e, f), while high concentrations of $H_2O$ improve the contrast on metal-based compounds like iron oxide (Fig. 2c, d). Consequently, SANS is a powerful technique for the characterization of core-shell structures such as iron-carbohydrate complexes. To perform a SANS contrast variation experiment, a series of scattering curves are measured, which are then analyzed independently. The curve, where the scattering length density of the iron core is matched with the scattering length density of the solvent, can be used to model the carbohydrate ligand. Likewise, the curve, where the scattering length density of the carbohydrate ligand is matched with the scattering length density of the solvent, can be used to model the iron core. In addition, the analysis and modeling of vastly different contrast profiles obtained from SANS may be used as a further input or verification for SAXS experiments of the same material, making it an optimal complementary technique (Sommer et al., 2005; Seelenmeyer et al., 2001). However, SANS is only accessible at large-scale facilities and provides a significantly lower flux compared to X-ray sources, which increases substantially the measurement time. SAXS and SANS are powerful tools to investigate the nanoscale structure of iron carbohydrate complexes. Hereby, SAXS is well suited to study the iron core due to its high contrast to the carbohydrate ligand and surrounding media, while SANS can complement to resolve the much lower contrast of the carbohydrate ligand. Both techniques can investigate iron carbohydrates in their native environment, but also in any condition including biological environments such as complex cell culture media and protein solutions (Li et al., 2016).

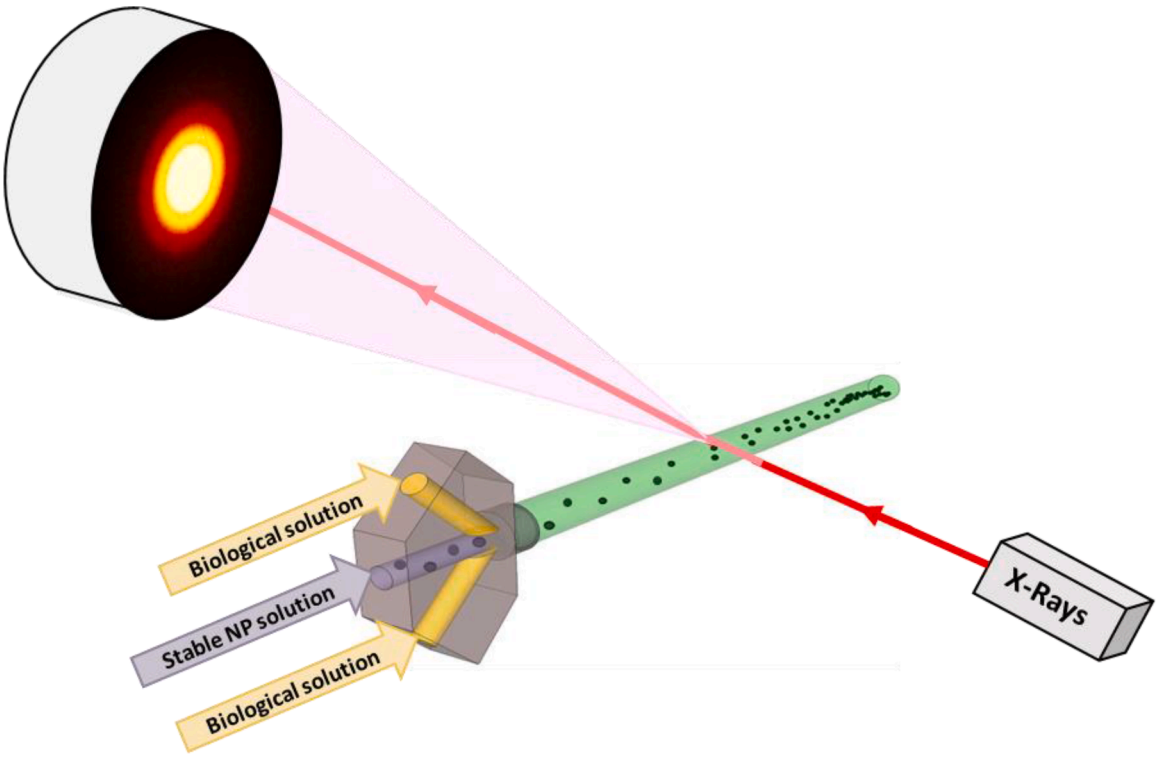


**Fig. 3.** Schematic representation of a SAXS set-up coupled with a microfluidic mixing system to perform time-resolved studies of nanoparticles in biological environments. Figure adapted and modified from Iranpour Anaraki et al. (2022).

### 6.3. *In-situ exposure to biological components*

The dynamic character of an intravenous injection of iron carbohydrate nanoparticles into the human bloodstream requires the need for *in-situ* studies. This is especially important as exposure of NPs to in vivo environments can induce agglomeration, dissolution and sedimentation due to changes in pH and ionic strength. Chemical alterations to the material due to the generation of radical oxygen species (ROS) and oxidative stress may also be possible (Pfeiffer et al., 2014). Exposure of NPs to biomolecules may change surface properties of the coating such as hydrophobicity, charge and roughness and could give the NP a completely new bio-identity by formation of a protein corona (Wang et al., 2011; Nel et al., 2009). Protein interactions may also affect the NP core, which would influence its shape-dependent characteristics as well as its size or distribution (Sanchez-Cano et al., 2021). Here, the use of micro- or nanofluidic devices coupled with SAXS could be a promising strategy as it would simulate *in-vivo* environments by resembling fluid flow conditions as observed in the body (Fig. 3). Changes in the agglomeration state, single NP size and shape, onset of sedimentation and interaction of NPs with biomolecules could be observed in real-time with different temperature or pH settings. This has been applied to investigate thermal decomposition and temperature-dependent agglomeration of oleic acid-coated iron oxide nanoparticles as well as formation of iron oxide compounds (Appel et al., 2021; Rose et al., 2014; Lassenberger et al., 2017). SAXS studies involving interaction of silica and gold NP with human serum albumin have also been performed, which enabled the determination of corona thickness and the number of agglomerated proteins (Wang et al., 2011; Anaraki et al., 2020; N Iranpour Anaraki et al., 2022; Spinozzi et al., 2017; N Iranpour Anaraki et al., 2022). Here, SANS may be especially advantageous if the specific interaction between the carbohydrate ligand and the protein of interest has to be investigated separately from the iron core (Wang et al., 2011; Anaraki et al., 2020; N Iranpour Anaraki et al., 2022; Spinozzi et al., 2017). Since neutrons do not damage proteins, SANS is also a better choice if radiation damage to sensible proteins needs to be avoided. If the specific carbohydrate-protein interactions need to be studied *in-situ*, a coupled SANS-microfluidic approach can be used (Adamo et al., 2017). After injection of iron carbohydrates into the (human) body, the study of the cellular uptake would be of importance. Accordingly, SAXS combined with a microfluidic setup could be used to monitor the nanoparticle uptake, as shown in dynamic studies of interactions between cubic liposomes and cells (Lam et al., 2020).

Some nanoparticulate systems like iron-carbohydrate complexes agglomerate when they are diluted. This can generate additional scattering contributions induced by formation of large structures and/or interactions between individual NPs, making analysis and proper modeling of SAXS data challenging. To solve this, one can measure the sample at different dilutions to pinpoint the onset of concentration-dependent agglomeration or inter-particle interactions, assuming that the structure of the individual NPs does not change upon dilution (Larsen and Pedersen, 2020). By dividing the SAXS data at the highest concentration through the SAXS data, where no agglomeration and inter-particle interactions are observed (non-interacting case), the structure of the agglomerates or the nature of the inter-particle interactions (e.g. electrostatic and excluded volume) can be determined. This analysis must be done with care as scattering contribution from agglomerates and inter-particle interactions are often intermingled. Using similar dilution factors when SAXS, XRD, DLS and cryo-TEM data are compared, is therefore highly important.

## 7. Discussion

Given the inherent complexity of iron-carbohydrate nanomedicines, it is clear that no single analytic testing approach can provide accurate information regarding the physical structure of these complex drug products. Several characterization technologies, including DLS and zeta potential, have advanced our understanding of the physicochemical characteristics of these nanoparticle drug products (Di Francesco and Borchard, 2018). However, there is currently an urgent unmet need to expand the constellation of analytical tests for iron-carbohydrate

nanoparticle products to evaluate this complex class of drugs (Brandis et al., 2021).

The entire iron-carbohydrate complex is necessary to function in the intended therapeutic manner (Funk and Barton, 2021; Wu et al., 2017; US FDA, 2022). Intravenous administration of polynuclear iron alone is associated with dose-limiting serious adverse events related to rapid increases in free iron (Goetsch and Moore, 1946). Thus, the polynuclear iron must be bound to the carbohydrate ligand such that the entire complex is safer, shuttled by macrophages that phagocytize the nanoparticles and transport them for safe storage in the MPS until the iron is mobilized for transport to the site of action (Funk and Barton, 2021). Analyses that are performed on the intact particle should not be replicated when iron is separated from the carbohydrate ligand. The entire iron-carbohydrate complex interfaces with the biological milieu, thus performing tests on iron extracted from the nanoparticle has no relevance to in vivo disposition. Moreover, performing certain analytical characterization on the iron core for example may be impossible due to stability challenges.

DLS has become the gold standard for particle size evaluation for regulatory agencies (Caputo et al., 2019). DLS can be used for the purpose of quickly measuring a high amount of samples. However, DLS measurements can be very sensitive to some parameters that need to be taken into consideration to ensure reproducible and comparable data. These parameters are described as number of replicate measurements, concentration of the nanoparticles, composition of the diluent, refractive index values of the nanoparticles and diluent, viscosity of the diluent, temperature of the measurement, type of cuvette, instrument model, scattering angle(s) and laser wavelength (Hackley, 2015). It is also important to pay attention to the type of algorithms used to calculate the size (Zou et al., 2017). According to (FDA) guidance for drug products containing nanomaterials, the size should be presented as average particle size (Z-average) and particle size distribution by the polydispersity index (PDI) and/or description of d10, d50, d90 (US_FDA 2022). It should be noted that performing DLS analysis on the polynuclear iron core alone would be expected to yield the hydrodynamic diameter of agglomerated iron cores rather than of a single iron core as removal of the stabilizing carbohydrate ligand will likely induce a fast collapse of the colloidal structure (Zou et al., 2017).

DLS fits very well as a routine analysis method for the detection of major issues with sample integrity and colloidal stability of iron-carbohydrate nanoparticles (Caputo et al., 2019). However, it might not be sensitive enough to accurately control the batch-to-batch variability. In addition, DLS alone is not able to distinguish larger particles from small aggregates or discriminate between different size populations of nanoparticles, or to evaluate the influence of biological environments on the average particle size and polydispersity. Therefore, complementary methods such as SEC, AF4, AF4 NP-sorting coupled with online sizing DLS and/or multi-angle light scattering (MALS), NTA, AUC, TRPS or other orthogonal sizing techniques, including SAXS, SANS or cryo-TEM can be used in combination with DLS to detect such small variations that may compromise their quality and can affect their pharmacological activity and metabolic fate.

The particle size and size distribution can be measured by TEM as well. Nonetheless, it is important to choose a statistically relevant number of particles in a TEM image and number of images to be able to perform comparative analyses (Zou et al., 2017). However, TEM only provides the physical characteristics of the core (e.g. size, size distribution and morphology), as the carbohydrate ligand cannot be determined due to a lack of contrast when using common staining protocols. On the other hand, DLS gives only particle size and size distribution information of the whole intact particles. So, both analyses can be complementary to each other. It is central to reinforce the importance of sample preparation, for example, cryo-TEM can preserve the native state and morphology of iron carbohydrate nanoparticles when compared to room-temperature TEM analysis because it avoids introduction of artifacts such as aggregation (Wu et al., 2016).

XRD also provides relevant information about size, morphology, and crystallinity of iron carbohydrate nanoparticles. However, the XRD technique alone is not conclusive enough in some cases due to poor crystallinity and even amorphous character of some iron-carbohydrate complexes (Zou et al., 2017). As XRD relates to the mean coherence lengths in a system (see above), a NP can be much larger than a crystallite. One NP may contain either a single crystallite or multiple crystallites. Also the fact that the surface of a particle can be amorphous contributes to the size difference determined by XRD (crystallite size) and other methods such as SAXS (NP size). Therefore, the use of additional techniques can complement the information on size, morphology, and crystallinity characterization of iron carbohydrates nanoparticles.

Mössbauer spectroscopy has the potential to overcome some of the limitations of XRD by providing information about iron speciation even when the iron phase is poorly crystalline. While using Mössbauer spectroscopy, it is important to consider limitations on (i) spectral quality and (ii) interpretation of spectral features. The signal-to-noise ratio of a spectrum depends on the absorption and emission of energy by $^{57}$Fe nuclei; therefore, the quantity of $^{57}$Fe present should be sufficient for a strong signal. At the natural abundance of $^{57}$Fe (2.1%), this requires several milligrams of Fe. Further, if the sample contains high concentrations of carbon, in this case carbohydrates, a larger sample

**Table 2**
Orthogonal methods that when used collectively assist in determining the physical structure of iron-carbohydrate nanoparticles.

| Analytical Technique | Iron-carbohydrate particle size | Iron-carbohydrate particle morphology | Iron core particle size | Iron core morphology/ crystallinity | Carbohydrate ligand |
|---|---|---|---|---|---|
| DLS | X (Di Francesco and Borchard, 2018) | | | | |
| Cryo-TEM | X (Wu et al., 2016) | X | X | X | |
| XRD | | | | X (Zou et al., 2017) | |
| AFM | X (Neiser et al., 2015) | X | | | |
| XANES | | | | X (Neiser et al., 2015) | |
| Size Exclusion | X (Jahn et al., 2011) | | | | |
| Mössbauer | | | X (Enver Murad, 2004) | X (crystallinity) (Neiser et al., 2015) | |
| SAXS | | | X (Appel et al., 2021; Rose et al., 2014; Lassenberger et al., 2017; Bonini et al., 2007) | | |
| SANS | X (Fu et al., 2016) | | X (Hore et al., 2013) | | X (thickness) (Diroll et al., 2015; Hore et al., 2013) |
| Zeta Potential | | | | | X (Jahn et al., 2011) |

**Table 3**
Regulatory recommendations from FDA (US_FDA 2022) and EMA (European_Medicines_Agency 2015) concerning quality aspects that need to be taken in consideration for the characterization of iron-carbohydrate nanoparticles and nanomedicines in general. The agencies have recognized the fundamental role of the 3-dimensional structure analysis in points 2, 3, 4, 6, 7 and 8.

| Quality recommendations | | |
|---|---|---|
| Item | US Food and Drug Administration's (FDA) | European Medicines Agency (EMA) |
| 1 | Chemical composition, Particle concentration, Porosity (if it relates to a function, e.g., capacity to load a drug) | Quality standard for carbohydrates used in the manufacture of the active substance and finished product (description, source and characterization, manufacture, assay, impurity profile, and stability characteristics), |
| 2 | Average particle size, Structural attributes that relate to function (e.g., lamellarity, core-shell structure) | Size of the iron core |
| 3 | Particle size distribution (PSD) (description of d10, d50, d90 or polydispersity; modality) (US_FDA September 2021) | Particle size, size distribution, charge, and surface properties of the iron-carbohydrate complexes |
| 4 | Stability, both physical (e.g., aggregation and agglomeration or separation) and chemical | Spectroscopic properties (e.g. 1H—NMR, 13C—NMR, IR, UV–VIS, MS, XRD), Stability on storage of the product |
| 5 | Assay of drug substance | Identification and control of key intermediates in the manufacturing process |
| 6 | General shape and morphology (aspect ratio), Surface properties (e.g., surface area, surface charge, chemical reactivity, ligands, hydrophobicity, and roughness) | Structure and composition of carbohydrate matrix, Morphology e.g. microscopic evaluation of the surface |
| 7 | Coating properties, including how coatings are bound to the nanomaterial | Ratio of bound carbohydrate to iron |
| 8 | Crystal form | Polymorphic form of the iron comprising the core |
| 9 | Impurities, Distribution of any drug substance associated with the nanomaterial and free in solution (e.g., surface bound or liposome encapsulated versus free drug substance) | Amount of labile iron released from the product when administered, Impurities e.g. ratio of divalent and trivalent iron |
| 10 | Biodegradability of the nanomaterials and their constituents, In vitro release | Degradation path for the iron-carbohydrate complex, where justified, a reliable and discriminating method for determining degradation kinetics should be developed (degradation in acid has previously been performed for some products). |
| 11 | Compatibility of the nanomaterial relevant to in-use conditions | In-use stability (including after reconstitution with recommended diluents for administration) with consideration to instructions for administration in the SmPC e.g. concentration |

mass may be required in order to overcome dampening of the signal due to organic carbon. In addition, the effects of crystallinity, particle size, and particle interactions need to be considered during the interpretation of doublets and sextets in sample spectra. Both crystallinity and particle size are related to the blocking temperature of a sample (Enver Murad, 2004); as a result, a low blocking temperature may reflect a low crystallinity phase or a small particle size. Therefore, complementary methods such as TEM and/or SAXS should be used in order to differentiate between the effect of crystallinity and particle size while comparing different iron carbohydrate nanoparticles. One drawback when using SAXS to describe the iron-carbohydrate complexes is the relative ambiguity of the collected data due to their high polydispersity. This means that multiple models are equally valid to characterize the same system. To get a more precise and physically meaningful model it is therefore to utmost importance to use additional techniques such as cryo-TEM, XRD and DLS to collect prior structural information (Pauw, 2014). For example, DLS and cryo-TEM data can be acquired as an input for polydispersity and shape of the particles, respectively, in order to obtain a precise solution for the size and arrangement of both single nanoparticles and their agglomerates. As an alternative approach, size and polydispersity can be estimated using XRD and cryo-TEM, respectively, to get a definite solution for the shape of the particles. One has to be cautious when comparing size parameters between SAXS and cryo-TEM as the equivalent diameter used in TEM assumes spherical objects and hence does not fully align with the average of the particle size determined via SAXS. The hydrodynamic diameter extracted from DLS is also often significantly higher compared to SAXS since size parameters do not take into account hydration of the nanoparticle (Pabisch et al., 2012; Vestergaard et al., 2005; Bron et al., 2008). X-ray fluorescence, due to absorption of X-rays by the iron atoms within iron carbohydrates, can lead to a high background signal, making proper interpretation of the SAXS data more difficult. Limiting the X-ray radiation to a narrow distribution of wavelengths by using monochromators (e.g. in synchrotron sources) can eliminate this issue. (Mos et al., 2018) Taken collectively, to achieve reliable information on size, shape and other structural parameters of iron carbohydrate nanoparticles, the benefits of different techniques have to be harnessed. While TEM provides real space images containing size and shape information, SAXS delivers data with high statistical relevance in solution conditions.

## Conclusion

Intravenous iron-carbohydrate nanomedicines are widely used across very broad and heterogenous patient populations (Auerbach and Ballard, 2010). More data are needed to evaluate the iron-carbohydrate complex's behavior in situ to better understand their physical structure at the nano-bio interface (Mahmoudi, 2021). The nanomedicine domain has made great strides in developing and validating new physicochemical characterization methods (e.g. DLS), however, these methods have limitations in providing relevant data to inform the three dimensional physical structure of iron-carbohydrate nanomedicines. Complementary use of orthogonal methods (e.g. Mössbauer spectroscopy, SAXS/SANS) offer greater insight into structural differences between the iron-carbohydrate nanomedicines. Therefore, when physicochemical characterization is applied, the determination of similarity in comparability assessments for bioequivalence evaluation, should include a validated collection of complementary orthogonal approaches.

## Author credit statement

The authors confirm contribution to the paper as follows: manuscript conception and design: BF, RD, AA, LK, draft manuscript preparation: BF, RD, AA, LK, PJ, AK. review and editing of manuscript: PW, AN All authors reviewed the results and approved the final version of the manuscript.

## Data availability

No data was used for the research described in the article.

## Acknowledgments

BF, AA and RD are employees of CSL Vifor
AK acknowledges infrastructural support by the Deutsche Forschungsgemeinschaft (DFG, German Research Foundation) under Germany's Excellence Strategy, cluster of Excellence EXC2124, project ID 390838134.

## References


Cappellini, M.D., Musallam, K.M., Taher, A.T., 2020. Iron deficiency anaemia revisited. J. Intern. Med. 287 (2), 153–170.

Richards, T., Breymann, C., Brookes, M.J., Lindgren, S., Macdougall, I.C., McMahon, L.P., et al., 2021. Questions and answers on iron deficiency treatment selection and the use of intravenous iron in routine clinical practice. Ann. Med. 53 (1), 274–285.

Auerbach, M., Ballard, H., 2010. Clinical use of intravenous iron: administration, efficacy, and safety. Hematol. Am. Soc. Hematol. Educ. Program 2010, 338–347.

Goetsch, A.T., Moore, C.V., 1946. Minnich V. Observations on the effect of massive doses of iron given intravenously to patients with hypochromic anemia. Blood 1, 129–142.

Funk, F.F., Barton, A., 2021. Criticality of surface characteristics of intravenous iron-carbohydrate nanoparticle complexes: implications for pharmacokinetics and pharmacodynamics. Int. J. Mol. Sci. 23 (4), 2140.

Funk, F., Weber, K., Nyffenegger, N., Fuchs, J.A., Barton, A., 2022. Tissue biodistribution of intravenous iron-carbohydrate nanomedicines differs between preparations with varying physicochemical characteristics in an anemic rat model. Eur. J. Pharm. Biopharm. 174, 56–76.

Garbowski, M.W., Bansal, S., Porter, J.B., Mori, C., Burckhardt, S., Hider, R.C., 2020. Intravenous iron preparations transiently generate non-transferrin-bound iron from two proposed pathways. Haematologica. Online ahead of print.

Aguera, M.L., Martin-Malo, A., Alvarez-Lara, M.A., Garcia-Montemayor, V.E., Canton, P., Soriano, S., et al., 2015. Efficiency of original versus generic intravenous iron formulations in patients on haemodialysis. PLoS ONE 10 (8), e0135967.

Rottembourg, J., Kadri, A., Leonard, E., Dansaert, A., Lafuma, A, 2011. Do two intravenous iron sucrose preparations have the same efficacy? Nephrol. Dial. Transplant. 26 (10), 3262–3267.

US_FDA. Draft guidance on ferric oxyhydroxide. September 2021.

Nikravesh, N., Borchard, G., Hofmann, H., Philipp, E., Fluhmann, B., Wick, P., 2020. Factors influencing safety and efficacy of intravenous iron-carbohydrate nanomedicines: from production to clinical practice. Nanomedicine 26, 102178.

US_FDA. Drug products, including biological products, that contain nanomaterials guidance for industry. 2022.

Marden, E., Ntai, I., Bass, S., Fluhmann, B., 2018. Correction to: reflections on FDA draft guidance for products containing nanomaterials: is the abbreviated new drug application (ANDA) a suitable pathway for nanomedicines? AAPS J. 20 (6), 104.

European_Medicines_Agency. Reflection paper on the data requirements for intravenous iron-based nano-colloidal products developed with reference to an innovator medicinal product 2015. https://wwwemaeuropaeu/en/documents/scientific-guideline/reflection-paper-data-requirements-intravenous-iron-based-nano-colloidal-products-developed_enpdf.accessed 12 December 2021.

Agency E.M. Note for guidance on biotechnological/biological products subject to changes in their manufacturing process (CPMP/ICH/5721/03). 2005.

Simon Jr., C.G., Borgos, S.E., Calzolai, L., Nelson, B.C., Parot, J., Petersen, E.J., et al., 2023. Orthogonal and complementary measurements of properties of drug products containing nanomaterials. J. Control Release 354, 120–127.

Dobrovolskaia, M.A., 2022. Lessons learned from immunological characterization of nanomaterials at the Nanotechnology Characterization Laboratory. Front. Immunol. 13, 984252.

Monopoli, M.P., Walczyk, D., Campbell, A., Elia, G., Lynch, I., Bombelli, F.B., et al., 2011. Physical-chemical aspects of protein corona: relevance to in vitro and in vivo biological impacts of nanoparticles. J. Am. Chem. Soc. 133 (8), 2525–2534.

Mahmoudi, M., 2021. The need for robust characterization of nanomaterials for nanomedicine applications. Nat. Commun. 12 (1), 5246.

Wu, M., Sun, D., Tyner, K., Jiang, W., Rouse, R., 2017. Comparative evaluation of U.S. brand and generic intravenous sodium ferric gluconate complex in sucrose injection: in vitro cellular uptake. Nanomaterials (Basel). 7 (12).

Fluhmann, B., Ntai, I., Borchard, G., Simoens, S., Nanomedicines, Muhlebach S., 2019. The magic bullets reaching their target? Eur. J. Pharm. Sci. 128, 73–80.

Pai, A.B., 2015. Evaluating plasma pharmacokinetics of intravenous iron formulations: judging books by their covers? Clin. Pharmacokinet. 54 (4), 323–324.

Lee, E.S., Park, B.R., Kim, J.S., Choi, G.Y., Lee, J.J., 2013. Lee IS. Comparison of adverse event profile of intravenous iron sucrose and iron sucrose similar in postpartum and gynecologic operative patients. Curr. Med. Res. Opin. 29 (2), 141–147.

Di Francesco, T., Sublet, E., Borchard, G., 2019. Nanomedicines in clinical practice: are colloidal iron sucrose ready-to-use intravenous solutions interchangeable? Eur. J. Pharm. Sci. 131, 69–74.

Lim, J., Yeap, S.P., Che, H.X., Low, S.C, 2013. Characterization of magnetic nanoparticle by dynamic light scattering. Nanoscale Res. Lett. 8 (1), 381.

Gioria, S., Caputo, F., Urbán, P., Maguire, C.M., Bremer-Hoffmann, S., Prina-Mello, A., et al., 2018. Are existing standard methods suitable for the evaluation of nanomedicines: some case studies. Nanomedicine 13 (5), 539–554.

Caputo, F., Clogston, J., Calzolai, L., Rösslein, M., Prina-Mello, A., 2019. Measuring particle size distribution of nanoparticle enabled medicinal products, the joint view of EUNCL and NCI-NCL. A step by step approach combining orthogonal measurements with increasing complexity. J. Control Release 299, 31–43.

Varenne, F., Makky, A., Gaucher-Delmas, M., Violleau, F., Vauthier, C., 2016. Multimodal dispersion of nanoparticles: a comprehensive evaluation of size distribution with 9 size measurement methods. Pharm. Res. 33 (5), 1220–1234.

Mehn, D., Caputo, F., Rösslein, M., Calzolai, L., Saint-Antonin, F., Courant, T., et al., 2017. Larger or more? Nanoparticle characterisation methods for recognition of dimers. RSC Adv 7 (44), 27747–27754.

Anderson, W., Kozak, D., Coleman, V.A., Jamting, A.K., Trau, M., 2013. A comparative study of submicron particle sizing platforms: accuracy, precision and resolution analysis of polydisperse particle size distributions. J. Colloid Interface Sci. 405, 322–330.

Di Francesco, T., Borchard, G., 2018. A robust and easily reproducible protocol for the determination of size and size distribution of iron sucrose using dynamic light scattering. J. Pharm. Biomed. Anal. 152, 89–93.

Süß, S., Metzger, C., Damm, C., Segets, D., Peukert, W., 2018. Quantitative evaluation of nanoparticle classification by size-exclusion chromatography. Powder Technol 339, 264–272.

Zou, P., Tyner, K., Raw, A., Lee, S., 2017. Physicochemical characterization of iron carbohydrate colloid drug products. AAPS J. 19 (5), 1359–1376.

Held, D., Kilz, P., 2021. Size-exclusion chromatography as a useful tool for the assessment of polymer quality and determination of macromolecular properties. Chem. Teacher Int. 3 (2), 77–103.

Wagner, M., Holzschuh, S., Traeger, A., Fahr, A., Schubert, U.S, 2014. Asymmetric flow field-flow fractionation in the field of nanomedicine. Anal. Chem. 86 (11), 5201–5210.

Yohannes, G., Jussila, M., Hartonen, K., Riekkola, M.L., 2011. Asymmetrical flow field-flow fractionation technique for separation and characterization of biopolymers and bioparticles. J. Chromatogr. A 1218 (27), 4104–4116.

Maguire, C.M., Rosslein, M., Wick, P., Prina-Mello, A., 2018. Characterisation of particles in solution - a perspective on light scattering and comparative technologies. Sci. Technol. Adv. Mater. 19 (1), 732–745.

Schuck, P., Zhao, H., Brautigam, C.A., Ghirlando, R., 2015. Basic Principles of Analytical Ultracentrifugation, 1st ed. CRC Press.

Walter, J., Löhr, K., Karabudak, E., Reis, W., Mikhael, J., Peukert, W., et al., 2014. Multidimensional analysis of nanoparticles with highly disperse properties using multiwavelength analytical ultracentrifugation. ACS Nano 8 (9), 8871–8886.

Weatherall, E., Willmott, G.R., 2015. Applications of tunable resistive pulse sensing. Analyst 140 (10), 3318–3334.

Jahn, M.R., Andreasen, H.B., Futterer, S., Nawroth, T., Schunemann, V., Kolb, U., et al., 2011. A comparative study of the physicochemical properties of iron isomaltoside 1000 (Monofer), a new intravenous iron preparation and its clinical implications. Eur. J. Pharm. Biopharm. 78 (3), 480–491.

Titus, D., James Jebaseelan Samuel, E., Roopan, S.M, 2019. Chapter 12 - Nanoparticle characterization techniques. In: Shukla, AK, Iravani, S (Eds.), Green Synthesis, Characterization and Applications of Nanoparticles. Elsevier, pp. 303–319.

Wu, Y., Petrochenko, P., Chen, L., Wong, S.Y., Absar, M., Choi, S., et al., 2016. Core size determination and structural characterization of intravenous iron complexes by cryogenic transmission electron microscopy. Int. J. Pharm. 505 (1–2), 167–174.

Kudasheva, D.S., Lai, J., Ulman, A., Cowman, M.K., 2004. Structure of carbohydrate-bound polynuclear iron oxyhydroxide nanoparticles in parenteral formulations. J. Inorg. Biochem. 98 (11), 1757–1769.

Monshi, A., 2012. Modified Scherrer equation to estimate more accurately nano-crystallite size using XRD. World J. Nano Sci. Eng. 2, 154–160.

Suryanarayana, C., Grant Norton, M., 1998. X-ray Diffraction: A Practical Approach. Springer, New York.

Bhattacharjee, S., 2016. DLS and zeta potential – What they are and what they are not? J. Controlled Release 235, 337–351.

Carvalho, P.M., Felício, M.R., Santos, N.C., Gonçalves, S., Domingues, M.M., 2018. Application of light scattering techniques to nanoparticle characterization and development. Front. Chem. 6.

Enver Murad, J.C, 2004. Mössbauer Spectroscopy of Environmental Materials and Their Industrial Utilization, 1 ed. Springer Science+Business Media, New York.

Mössbauer, R.L., 1958. Kernresonanzabsorption von Gammastrahlung in Ir191. Naturwissenschaften 45 (22), 538–539.

Coey, J.M.D, 1984. Mössbauer Spectroscopy of Silicate Minerals. Mössbauer Spectroscopy Applied to Inorganic Chemistry. Springer US, pp. 443–509. G. J. Long. Boston, MA.

Thompson, A., Rancourt, D.G., Chadwick, O.A., Chorover, J., 2011. Iron solid-phase differentiation along a redox gradient in basaltic soils. Geochim. Cosmochim. Acta 75 (1), 119–133.

Neiser, S., Rentsch, D., Dippon, U., Kappler, A., Weidler, P.G., Gottlicher, J., et al., 2015. Physico-chemical properties of the new generation IV iron preparations ferumoxytol, iron isomaltoside 1000 and ferric carboxymaltose. Biometals 28 (4), 615–635.

Byrne, J.M., Kappler, A., 2022. A revised analysis of ferrihydrite at liquid helium temperature using Mössbauer spectroscopy. Am. Mineral. 107 (8), 1643–1651.

ThomasArrigo, L.K., Byrne, J.M., Kappler, A., Kretzschmar, R., 2018. Impact of organic matter on iron(II)-catalyzed mineral transformations in ferrihydrite–organic matter coprecipitates. Environ. Sci. Technol. 52 (21), 12316–12326.

Thompson, A., Chadwick, O.A., Rancourt, D.G., Chorover, J., 2006. Iron-oxide crystallinity increases during soil redox oscillations. Geochim. Cosmochim. Acta 70 (7), 1710–1727.

Latta, D.E., Bachman, J.E., Scherer, M.M., 2012. Fe electron transfer and atom exchange in goethite: influence of Al-substitution and anion sorption. Environ. Sci. Technol. 46 (19), 10614–10623.

Murad, E., 1984. High-precision determination of magnetic hyperfine fields by Mossbauer spectroscopy using an internal standard. J. Phys. E 17 (9), 736.

Schnablegger, H.S.Y, 2013. The SAXS Guide Getting Acquainted with the Principles, 3rd ed. AntonPaar GmbH, Graz, Austria.

Pauw, B.R., 2014. Corrigendum: everything SAXS: small-angle scattering pattern collection and correction, 2013J. Phys.: Condens. Matter 25 383201 J. Phys. Condens. Matter 26 (23), 239501.

Parra-Ortiz, E., Malekkhaiat Häffner, S., Saerbeck, T., Skoda, M.W.A., Browning, K.L., Malmsten, M, 2020. Oxidation of polyunsaturated lipid membranes by photocatalytic titanium dioxide nanoparticles: role of pH and salinity. ACS Appl. Mater. Interfaces 12 (29), 32446–32460.

Hassett, K.J., Higgins, J., Woods, A., Levy, B., Xia, Y., Hsiao, C.J., et al., 2021. Impact of lipid nanoparticle size on mRNA vaccine immunogenicity. J. Control Release 335, 237–246.
Aljuaid, N., Tully, M., Seitsonen, J., Ruokolainen, J., Hamley, I.W., 2021. Benzene tricarboxamide derivatives with lipid and ethylene glycol chains self-assemble into distinct nanostructures driven by molecular packing. Chem. Commun. 57 (67), 8360–8363.
Jouault, N., Dalmas, F., Said, S., Di Cola, E., Schweins, R., Jestin, J., et al., 2010. Direct small-angle-neutron-scattering observation of stretched chain conformation in nanocomposites: more insight on polymer contributions in mechanical reinforcement. Phys. Rev. E Stat. Nonlin. Soft Matter Phys. 82 (3 Pt 1), 031801.
Räntzsch V, Ö.M., Ratzsch, K.F., Stellamanns, E., Sprung, M., Guthausen, G., Wilhelm, M, 2019. Polymer crystallization studied by hyphenated rheology techniques: rheo-NMR, Rheo-SAXS, and rheo-microscopy. Macromol. Mater. Eng. 302.
Amirkhani, M., Sharifi, S., Funari, S.S., Marti, O., 2014. Depletion-induced sphere-cylinder transition in C12E5 microemulsion: a small-angle X-ray scattering study. Mol. Phys. 112 (12), 1702–1709.
Mahrhauser, D.S., Kählig, H., Partyka-Jankowska, E., Peterlik, H., Binder, L., Kwizda, K., et al., 2015. Investigation of microemulsion microstructure and its impact on skin delivery of flufenamic acid. Int. J. Pharm. 490 (1–2), 292–297.
Doblas, D., Kister, T., Cano-Bonilla, M., González-García, L., Kraus, T., 2019. Colloidal solubility and agglomeration of apolar nanoparticles in different solvents. Nano Lett. 19 (8), 5246–5252.
Huang, L., Mai, J., Zhu, Q., Guo, Z., Qin, S., Yang, P., et al., 2019. Reversible rearrangement of magnetic nanoparticles in solution studied using time-resolved SAXS method. J. Synchrotron Radiat. 26 (Pt 4), 1294–1301.
Appel, C., Kuttich, B., Stühn, L., Stark, R.W., Stühn, B., 2019. Structural properties and magnetic ordering in 2D polymer nanocomposites: existence of long magnetic dipolar chains in zero field. Langmuir 35 (37), 12180–12191.
Grünewald, T.A., Lassenberger, A., van Oostrum, P.D., Rennhofer, H., Zirbs, R., Capone, B., et al., 2015. Core-shell structure of monodisperse poly(ethylene glycol)-grafted iron oxide nanoparticles studied by small-angle X-ray scattering. Chem. Mater. 27 (13), 4763–4771.
Rasmussen, H.Ø., Wollenberg, D.T.W., Wang, H., Andersen, K.K., Oliveira, C.L.P., Jørgensen, C.I., et al., 2022. The changing face of SDS denaturation: complexes of Thermomyces lanuginosus lipase with SDS at pH 4.0, 6.0 and 8.0. J. Colloid Interface Sci. 614, 214–232.
Lenton, S., Hervø-Hansen, S., Popov, A.M., Tully, M.D., Lund, M., Skepö, M., 2021. Impact of Arginine-Phosphate Interactions on the Reentrant Condensation of Disordered Proteins. Biomacromolecules 22 (4), 1532–1544.
Hammouda, B, 2008. Probing Nanoscale Structures –The Sans Toolbox. National Institute of Standards and Technology.
Diroll, B.T., Weigandt, K.M., Jishkariani, D., Cargnello, M., Murphy, R.J., Hough, L.A., et al., 2015. Quantifying "softness" of organic coatings on gold nanoparticles using correlated small-angle X-ray and neutron scattering. Nano Lett. 15 (12), 8008–8012.
Rübe, A., Hause, G., Mäder, K., Kohlbrecher, J., 2005. Core-shell structure of Miglyol/poly(D,L-lactide)/Poloxamer nanocapsules studied by small-angle neutron scattering. J. Control Release 107 (2), 244–252.
Sommer, C., Pedersen, J.S., Garamus, V.M., 2005. Structure and interactions of block copolymer micelles of Brij 700 studied by combining small-angle X-ray and neutron scattering. Langmuir 21 (6), 2137–2149.
Seelenmeyer, S.D.I, Rosenfelt, S., Norhausen, C., Dingenouts, N., 2001. Ballauff M Small-angle x-ray and neutron scattering studies of the volume phase transition in thermosensitive core–shell colloids. J. Chem. Phys. 114, 10471.
Li, T., Senesi, A.J., Lee, B., 2016. Small angle X-ray scattering for nanoparticle research. Chem. Rev. 116 (18), 11128–11180.
Pfeiffer, C., Rehbock, C., Hühn, D., Carrillo-Carrion, C., de Aberasturi, D.J., Merk, V., et al., 2014. Interaction of colloidal nanoparticles with their local environment: the (ionic) nanoenvironment around nanoparticles is different from bulk and determines the physico-chemical properties of the nanoparticles. J. R. Soc. Interface 11 (96), 20130931.
Wang, J., Jensen, U.B., Jensen, G.V., Shipovskov, S., Balakrishnan, V.S., Otzen, D., et al., 2011. Soft interactions at nanoparticles alter protein function and conformation in a size dependent manner. Nano Lett. 11 (11), 4985–4991.
Nel, A.E., Mädler, L., Velegol, D., Xia, T., Hoek, E.M., Somasundaran, P., et al., 2009. Understanding biophysicochemical interactions at the nano-bio interface. Nat. Mater. 8 (7), 543–557.
Sanchez-Cano, C., Alvarez-Puebla, R.A., Abendroth, J.M., Beck, T., Blick, R., Cao, Y., et al., 2021. X-ray-based techniques to study the nano-bio interface. ACS Nano 15 (3), 3754–3807.
Appel, C., Kuttich, B., Kraus, T., Stühn, B., 2021. In situ investigation of temperature induced agglomeration in non-polar magnetic nanoparticle dispersions by small angle X-ray scattering. Nanoscale 13 (14), 6916–6920.
Rose, A.L., Bligh, M.W., Collins, R.N., Waite, T.D., 2014. Resolving early stages of homogeneous iron(III) oxyhydroxide formation from iron(III) nitrate solutions at pH 3 using time-resolved SAXS. Langmuir 30 (12), 3548–3556.
Lassenberger, A., Grünewald, T.A., van Oostrum, P.D.J., Rennhofer, H., Amenitsch, H., Zirbs, R., et al., 2017. Monodisperse iron oxide nanoparticles by thermal decomposition: elucidating particle formation by second-resolved in situ small-angle X-ray scattering. Chem. Mater. 29 (10), 4511–4522.
Anaraki, N.I., Sadeghpour, A., Iranshahi, K., Toncelli, C., Cendrowska, U., Stellacci, F., et al., 2020. New approach for time-resolved and dynamic investigations on nanoparticles agglomeration. Nano Res. 13 (10), 2847–2856.
Iranpour Anaraki, N., Liebi, M., Ong, Q., Blanchet, C., Maurya, A.K., Stellacci, F., et al., 2022a. In-situ investigations on gold nanoparticles stabilization mechanisms in biological environments containing HSA. Adv. Funct. Mater. 32 (9), 2110253.
Spinozzi, F., Ceccone, G., Moretti, P., Campanella, G., Ferrero, C., Combet, S., et al., 2017. Structural and thermodynamic properties of nanoparticle-protein complexes: a combined SAXS and SANS study. Langmuir 33 (9), 2248–2256.
Iranpour Anaraki, N., Liebi, M., Iranshahi, K., Blanchet, C., Wick, P., Neels, A., 2022b. Time-resolved study on self-assembling behavior of PEGylated gold nanoparticles in the presence of human serum albumin: a system for nanomedical applications. ACS Appl. Nano Mater. 5 (12), 18921–18929.
Adamo, M., Poulos, A.S., Miller, R.M., Lopez, C.G., Martel, A., Porcar, L., et al., 2017. Rapid contrast matching by microfluidic SANS. Lab Chip 17 (9), 1559–1569.
Lam, Y.Y., Hawley, A., Tan, A., Boyd, B.J., 2020. Coupling in vitro cell culture with synchrotron SAXS to understand the bio-interaction of lipid-based liquid crystalline nanoparticles with vascular endothelial cells. Drug Deliv. Transl. Res. 10 (3), 610–620.
Larsen, A.H., Pedersen, J.S., Arleth, L., 2020. Assessment of structure factors for analysis of small-angle scattering data from desired or undesired aggregates. J. Appl. Crystallogr. 53 (4), 991–1005.
Brandis, J.E.P., Kihn, K.C., Taraban, M.B., Schnorr, J., Confer, A.M., Batelu, S., et al., 2021. Evaluation of the physicochemical properties of the iron nanoparticle drug products: brand and generic sodium ferric gluconate. Mol. Pharm. 18 (4), 1544–1557.
Administration UFaD. Sameness Evaluations in an ANDA —Active Ingredients Guidance for Industry. 2022.
Hackley, V.A .CJ, 2015. Measuring the size of nanoparticles in aqueous media using batch-mode dynamic light scattering. NIST Spec. Publ. 1200–1206.
Pabisch, S., Feichtenschlager, B., Kickelbick, G., Peterlik, H., 2012 [Not Available] Chem. Phys. Lett. 521 (C), 91–97.
Vestergaard, B., Sanyal, S., Roessle, M., Mora, L., Buckingham, R.H., Kastrup, J.S., et al., 2005. The SAXS solution structure of RF1 differs from its crystal structure and is similar to its ribosome bound cryo-EM structure. Mol. Cell 20 (6), 929–938.
Bron, P., Giudice, E., Rolland, J.P., Buey, R.M., Barbier, P., Díaz, J.F., et al., 2008. Apo-Hsp90 coexists in two open conformational states in solution. Biol. Cell. 100 (7), 413–425.
Mos, Y.M.V., Arnold, C., Buisman, Cees J.N., Weijma, Jan;, 2018. X-ray diffraction of iron containing samples: the importance of a suitable configuration. Geomicrobiol. J. 35 (6), 511–517.
Bonini, M., Fratini, E., Baglioni, P., 2007. SAXS study of chain-like structures formed by magnetic nanoparticles. Mater. Sci. Eng.: C 27 (5), 1377–1381.
Fu, Z., Xiao, Y., Feoktystov, A., Pipich, V., Appavou, M.S., Su, Y., et al., 2016. Field-induced self-assembly of iron oxide nanoparticles investigated using small-angle neutron scattering. Nanoscale 8 (43), 18541–18550.
Hore, M.J.A., Ford, J., Ohno, K., Composto, R.J., Hammouda, B., 2013. Direct measurements of polymer brush conformation using small-angle neutron scattering (SANS) from highly grafted iron oxide nanoparticles in homopolymer melts. Macromolecules 46 (23), 9341–9348.